Preliminary investigation of seismic site conditions in Whitehorse (Kwänlin), Yukon, from passive seismic methods

*Jamie Friesen Byer**
Department of Earth, Energy, and Environment, University of Calgary

Jeremy M. Gosselin
Natural Resources Canada, Geological Survey of Canada–Pacific

Jan Dettmer
Yukon Geological Survey

Hersh Gilbert
Department of Earth, Energy, and Environment, University of Calgary

Byer, J.F., Gosselin, J.M., Dettmer, J. and Gilbert, H., 2026. Preliminary investigation of seismic site conditions in Whitehorse (Kwänlin), Yukon, from passive seismic methods. *In*: Yukon Exploration and Geology 2025, A. Stuart, L.H. Weston and S.K. Schultz (eds.), Yukon Geological Survey, Government of Yukon, p. 119–130.

Abstract

Although southwestern Yukon is tectonically active, with large historical and instrumentally recorded earthquakes, the seismic hazard in this region remains understudied compared to other regions of Canada. Ground shaking is influenced by source, path, and local geological effects, and local site conditions control the amplification and resonance of seismic energy. In this study, we use passive seismic recordings to constrain the seismic properties of the sediment for two sites in the Whitehorse (Kwänlin) area. Frequency-wavenumber beamforming is applied to ambient seismic noise from each site to extract surface-wave dispersion curves that contain information on sediment rigidity and subsurface structure. These dispersion curves are then used in a probabilistic inversion to determine one-dimensional shear-wave velocity models and associated uncertainties. Our results indicate that both sites are associated with seismic site class D, stiff soil. The results of this study improve the understanding of local seismic hazards in Kwänlin, lay the foundation for ongoing local seismic hazard investigations, and contribute to geohazard mitigation for northern Canada.

Plain language summary

Southwestern Yukon experiences large earthquakes, but these events have not been studied as extensively as those in other parts of Canada. The strength of earthquake ground shaking is influenced by the type of earthquake and by the ground materials—rock or sediment—beneath the surface. In this study, we use recordings of background Earth vibrations to measure sediment properties at two sites in the Whitehorse (Kwänlin) area. This information is useful for anticipating the severity of ground shaking during future earthquakes. Our results indicate that both sites can be classified as leading to a moderate increase in shaking severity compared to sites underlain with hard rock. These site classifications are used in building and infrastructure design under Canada's building code. Our work provides a step toward an improved understanding of natural hazards in Kwänlin, and lays a foundation for ongoing studies of regional sediment properties and local earthquake shaking hazards. Ultimately, this contributes to geohazard mitigation for northern Canada.

* jamie.byer@ucalgary.ca

Introduction

Whitehorse, Yukon, has an elevated risk of geohazards due to nearby active tectonics and rapid geomorphic processes. Northern communities such as Whitehorse also experience greater impacts of climate change as northern climates warm at more than double the global rate (Government of Yukon, 2022). Furthermore, a changing climate modulates geomorphic processes and can locally exacerbate geohazards (e.g., Dutta et al., 2008). Yukon is experiencing permafrost thaw, as well as more severe precipitation and wildfires (Government of Yukon, 2022). These can contribute to erosion, subsidence, landslides and increased severity of earthquake-induced ground shaking (Sun et al., 2017). Since spring 2022, multiple large landslides have occurred along the steep bluff that separates the Whitehorse airport from the downtown city centre (Brideau et al., 2024). These landslides caused disruptions to infrastructure and community access (Proulx, 2022), and highlight the need to better understand geohazards across Whitehorse to improve mitigation and community resilience.

The tectonics in southwestern Yukon are driven by the Yakutat microplate colliding and subducting beneath the North American plate (Bruhn et al., 2012; Gosselin et al., 2024). These active tectonics lead to rapid mountain building, erosion and earthquake activity (Fig. 1). Yukon is one of the most seismically active regions in Canada and has historically experienced numerous earthquakes of magnitude 6 and greater (Hyndman et al., 2005; Fig. 1). Seismicity from the nearby active Denali and Tintina faults (Eberhart-Phillips et al., 2003; Blais-Stevens et al., 2020; Biegel et al., 2024; Finley, 2025; Finley et al., 2025), as well as from the active plate boundary a few hundred kilometres to the southwest (Plafker, 1970; Doser, 2006), present significant additional hazards to the region. Geologically, the Yukon is part of the northern Canadian Cordillera, which formed through the accretion of magmatic arcs, continental arcs and oceanic basins onto the western margin of North America (Nelson et al., 2007). These accreted terranes have distinct geologic histories and are bounded by several large-scale faults (Kellett et al., 2017), mentioned above.

Earthquake hazards depend on the type and location of an earthquake, the propagation path of seismic energy, and local geological conditions (e.g., Kolaj et al., 2020). The Whitehorse trough sedimentary basin formed through accretion and was infilled by erosion during the Jurassic Period (White et al., 2012; van Drecht et al., 2022). Subsequent intrusive and volcanic activity produced plutonic and volcanic rocks that are now present in the subsurface. Because Whitehorse is proximal to several fault systems capable of generating large earthquakes, three-dimensional sedimentary basin structures that trap and amplify seismic energy are expected to influence ground motions in the area (e.g., Bard and Bouchon, 1980). The structure and properties of the sedimentary basin, its intrusions, and the contrast with the underlying crystalline basement may therefore exacerbate seismic hazard. Consequently, any knowledge on the seismic properties of rocks and sediments in the Whitehorse trough will improve our understanding of earthquake hazards.

At a local scale, earthquake shaking intensity and duration can be amplified by unconsolidated materials overlying bedrock due to resonance and seismic wave amplification (Anderson et al., 1986; Anderson et al., 1996), commonly referred to as seismic site effects. This study focuses on site effects associated with unconsolidated sediments and shallow bedrock within the upper ~100 m of the subsurface. In the Whitehorse area, unconsolidated sediments are predominantly less than 100 m thick and bedrock outcrops are sparse (Witter, 2025). These sediments were deposited during the McConnell Glaciation and include fine-grained silt and clay deposited in Glacial Lake Laberge (Lipovsky, 2023). The presence of these unconsolidated sediments of low rigidity overlying bedrock, combined with regional seismicity, has the potential to significantly increase the local seismic hazard.

The shear-wave velocity (V_S) is often used as a proxy for the rigidity of the soil/sediment at a site when evaluating conditions for earthquake engineering purposes. Specifically, the time-average V_S of the upper 30 m beneath a site (V_{S30}) is a useful parameter for the quantification of earthquake hazards. Furthermore, the National Seismic Hazard Model of Canada (Kolaj et al., 2020) assigns six specific site classes according to V_{S30} values measured or inferred at a site (Table 1). This allows for a more accurate application of the the National Building Code of Canada and highlights the importance of mapping near-surface geophysical properties throughout the Whitehorse area.

In this work, we used passive seismic recordings collected from two locations in Whitehorse to infer the one-dimensional (1D) near-surface Earth structure. Specifically, we apply frequency-wavenumber (f-k) beamforming to the ambient seismic noise recordings to extract surface-wave dispersion curves. The dispersion curves are then inverted using probabilistic

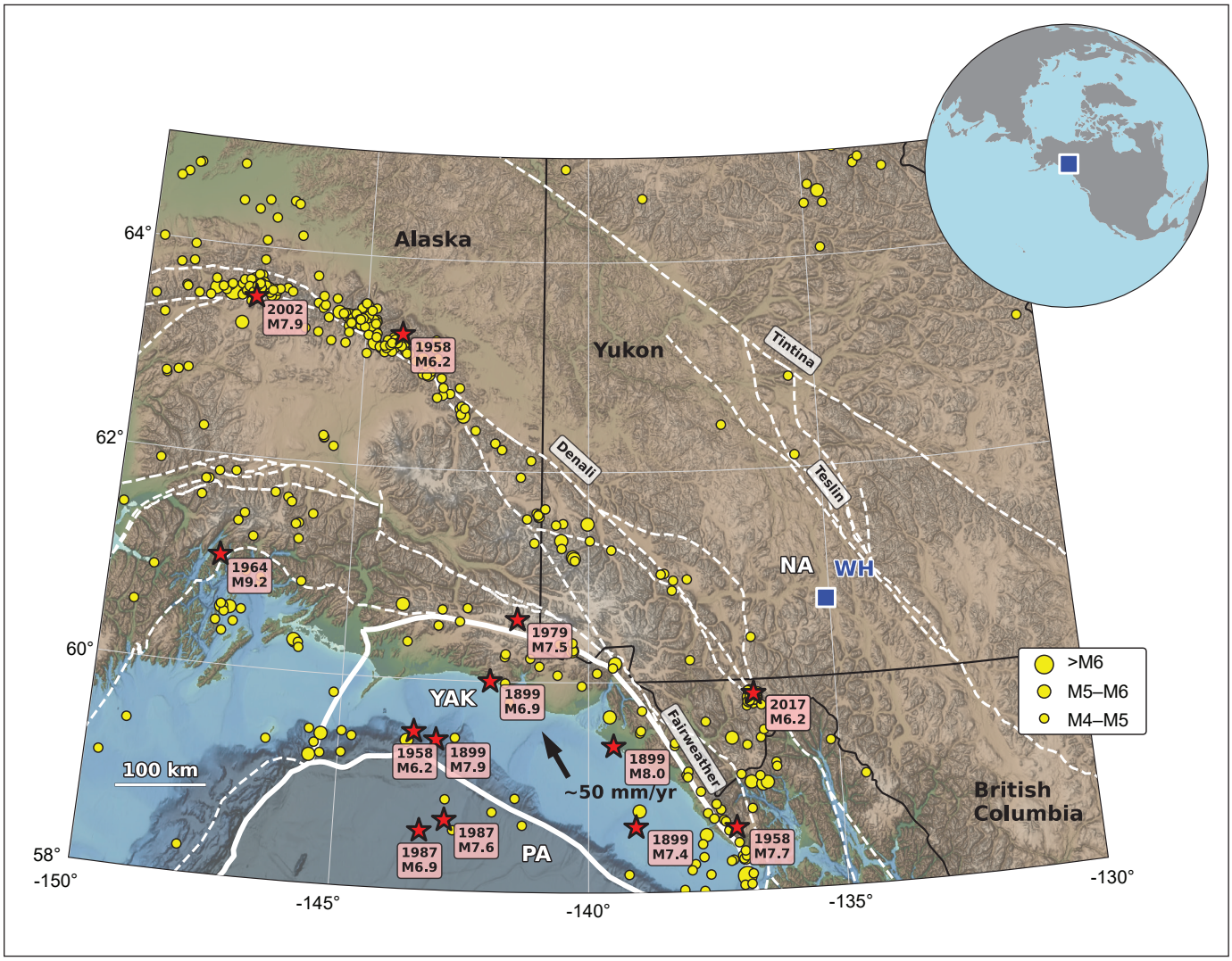

Figure 1. *Contributions to seismic hazards in southwestern Yukon. Instrumentally recorded earthquake epicentres (2000–2024) with magnitude ≥4 are represented by yellow circles, and significant earthquakes are represented by red stars. Major regional faults are indicated by dashed white lines, and the boundaries of the Pacific (PA), North American (NA), and Yakutat (YAK) tectonic plates are indicated by solid white lines. Provincial and territorial boundaries are marked with solid black lines. The location of Whitehorse (WH) is marked by the blue square.*

methods to estimate V_S profiles. Finally, the probability distributions of the V_{S30} values are determined from the inversion results and used to classify earthquake site hazards. The results of this work help improve the understanding of local seismic hazards in Whitehorse and lay the foundation for future microzonation analyses to understand the local variability in seismic hazards throughout the city and surrounding area. Ultimately, this will contribute to greater resilience of both the community and its infrastructure to geohazards.

Data and methods

Passive seismic array recordings

The passive seismic data used in this study were recorded on July 6, 2023 at two sites in the Whitehorse area (Fig. 2). Site A is in an agricultural field located along the Alaska Highway, approximately 20 km west of downtown Whitehorse, and site B is on a baseball field within the city limits. At each site, 14 Nanometrics Trillium Compact 120s broadband seismometers with Taurus seismographs were deployed in a cross-shaped configuration with a maximum station separation of approximately 100 m. The spacing between

instruments within the array increases outward, ranging from 5 to 45 m. This allows multiple and wider array apertures to collect data from a wider frequency band (Wathelet et al., 2008; Gosselin et al., 2018). These array apertures were chosen to target dispersion measurements over a specific frequency band that is sensitive to near-surface V_S over the depth extent that is relevant to seismic site amplification assessment (i.e., targeting the uppermost tens of metres).

The two site locations were selected based on several factors, including sufficient area to conduct passive seismic surveys, accessibility and relatively flat topography. In order to couple the seismometer to the ground, surface vegetation was removed beneath some instrument locations prior to installation. In addition, soft surficial materials beneath some instruments required that a ceramic tile be laid beneath seismometers to accurately level them. At site B, located on a baseball field, sufficient direct ground coupling could be achieved without tiles for all instruments. Synchronous ambient noise was collected on all instruments for approximately one hour with a sampling frequency of 100 Hz.

Table 1. The V_{S30} site classification used in Canada's national seismic hazard model (Kolaj et al., 2020).

Site class	Description	V_{S30} (m/s)
A	hardrock	1500
B	rock	760–1500
C	very dense soil and soft rock	360–760
D	stiff soil	180–360
E	soil with soft clay	<180
F	site-specific analysis required	—

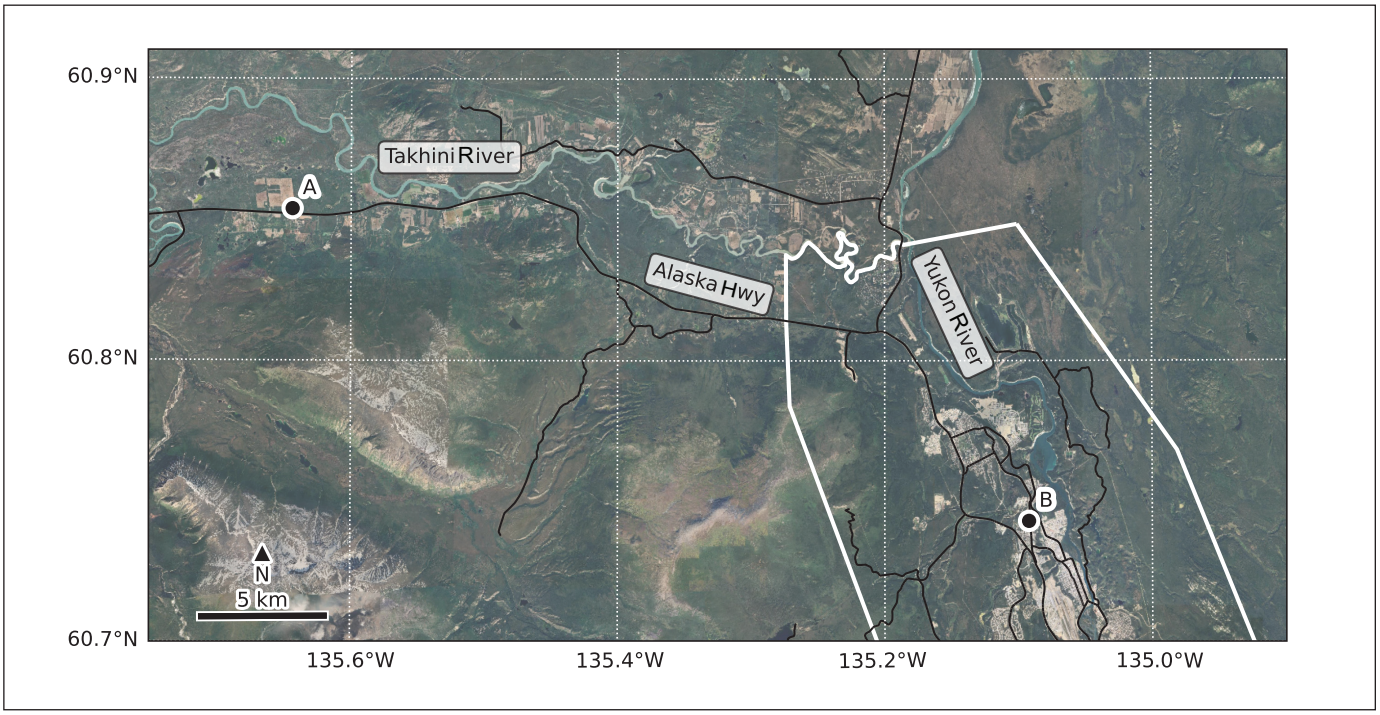

Figure 2. *The study area includes two focus site locations (labeled A and B). Whitehorse city limits (white lines), major roads (black lines) and rivers are also indicated.*

Frequency-wavenumber beamforming

The synchronous ambient seismic noise recordings were processed using Geopsy software (Wathelet et al., 2020) to perform frequency-wavenumber (f-k) beamforming and obtain fundamental-mode Rayleigh wave phase velocities as a function of frequency (i.e., dispersion). This beamforming approach estimates the propagation direction and speed of the dominant seismic signal propagating across the seismic array. The ambient seismic noise recordings are split into frequency-dependent time windows. For each time window, the beam power is calculated for a range of speeds and directions at the given frequency. The velocity with the maximum beam power is recorded for each time window, and this procedure is repeated for all time windows and all frequencies. The result is a distribution of phase velocities for each frequency.

The f-k beamforming analysis was performed for approximately 100 logarithmically-spaced frequencies between 1 and 15 Hz, assuming a phase velocity search grid between 200 and 2000 m/s. The approximately 1 hour of ambient seismic noise was divided into time windows with a frequency-dependent duration of 10 periods, with an overlap of 50%. Figure 3 illustrates the f-k beamforming results for all time windows and all frequencies, as well as the manually selected dispersion measurements retained for further analysis. Specifically, the dispersion data are taken as the median phase velocity of the time windows at each frequency. Measurement errors are taken to be the standard deviation at each frequency.

For site A, the dispersion curve is taken between 2.25 and 14.6 Hz, and for site B it is between 2.02 and 3.67 Hz and between 6.66 and 12.75 Hz. These frequency ranges were manually selected based on visual inspection of the f-k beamforming results and are frequencies where f-k results suggest sufficient constraint on phase velocity. These frequency limitations are likely due to a combination of site complexity, as well as the resolution and aliasing limits of the passive seismic array, which are dependent on the geometry and configuration of the array (Wathelet et al., 2008). For site A, at frequencies between about 5 and 8 Hz, and for site B at frequencies above approximately 10 Hz, phase velocities are near the lower processing bound of 200 m/s. Future work will investigate whether slower phase velocities, at higher frequencies, can be measured at these sites without the processing-imposed cutoff of our initial f-k beamforming analysis. For site B, at frequencies

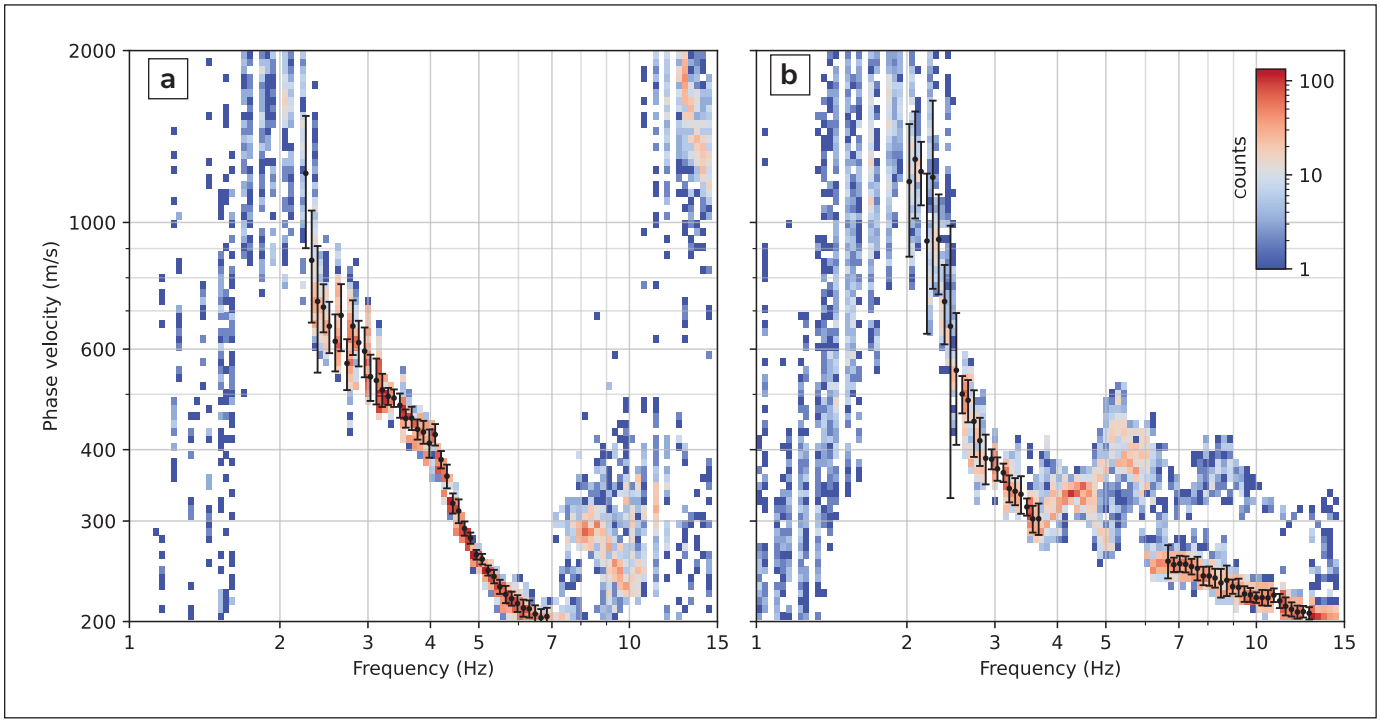

Figure 3. *Phase velocity dispersion from frequency-wavenumber (f-k) beamforming for* ***(a)*** *site A and* ***(b)*** *site B. Frequencies are chosen to be equidistant in log-space. Median phase velocities (black circles) and the standard deviations in phase velocity (error bars) are displayed, and represent the dispersion measurements used in subsequent analysis. The number of counts per bin are also illustrated by the colourbar.*

greater than 6.6 Hz, multiple phase velocity modes appear in the f-k results. At these frequencies, we qualitatively identify and remove the higher velocities associated with the second mode, which could bias our measurements (including the measurement errors). For site B, we exclude measurements between approximately 4 and 6 Hz due to the likely non-physical characteristics of the dispersion curve, which is expected to be smooth and nearly monotonic for phase velocities across frequencies. Further analysis is required to determine the cause of this processing result, though we speculate it may be partially due to the ambient seismic noise field during our 1-hour experiment. The final dispersion measurement selections for both sites suggest differences in near-surface site conditions.

Probabilistic inversion

Rayleigh wave dispersion is strongly dependent on V_S, and has a lesser sensitivity to density (ρ) and compressional-wave velocity (V_ρ; Xia et al., 1999). Consequently, dispersion curves can be used to infer V_S, and thereby the structure of the subsurface (Gosselin et al., 2022). For this problem, we parameterize the 1D Earth as a stack of layers over an infinite half-space, with unknown thicknesses and V_S. We determine V_ρ from V_S using a fixed V_ρ / V_S ratio of 1.75, and ρ using an empirical relation to V_ρ (Gardner et al., 1974). Since there are finite data, and these data have uncertainties, the inverse problem is non-unique, and many models can fit the data appropriately. In addition, the inverse problem is nonlinear as the sensitivity of the data to V_S depends on the model itself. To estimate 1D profiles of V_S from the computed dispersion curves and their uncertainties, we employ a probabilistic (Bayesian) Markov chain Monte Carlo (McMC) method (Molnar et al., 2010; Gosselin et al., 2022).

A posterior probability density (PPD) of the model parameters is estimated from a large ensemble of McMC samples dependent on the prior distribution, and on the data via a likelihood function. In this work, we assume that the prior distribution of the model parameters is uniform over a wide range of physically plausible values. The model parameters we infer are layer thicknesses and V_S. For both sites, we performed probabilistic inversions assuming several possible numbers of layers in the model. These inversions yielded similar results, leading us to qualitatively select a model consisting of three layers (two layers over a half-space) as the model with the minimum complexity required to explain our data. The prior bounds for the model parameters were chosen to be wide, yet physically plausible, to allow flexibility in the range of possible models that could be inferred to explain the data (Table 2). We used disba (Luu, 2024), a python implementation of Computer Programs in Seismology (Herrmann, 2013), to perform forward calculations that predict dispersion data for McMC model samples to evaluate model likelihood (i.e., data misfit). In this work, we assume a multi-variate Gaussian likelihood, with data errors at each frequency assumed to be independent and fixed to our measurement errors based on f-k processing (discussed above).

Results

Figure 4 displays the results of our passive seismic analysis for the data collected at site A. For illustration purposes, the figure bounds indicate the most pertinent region of the model and do not reflect the entire allowable prior model space. The configuration of the passive seismic array is delineated in Figure 4a, which highlights the extent (aperture) and configuration of the instruments deployed at the agricultural field site. We note that the minimum and maximum instrument separation distances are approximately 5 and 100 m, respectively. Figure 4b indicates the fit between the measured and predicted phase velocity dispersion data. Generally, the data predictions fall within the error bars for the field observations. The errors are larger for low frequencies, and this is reflected in the larger range in data predictions for low frequencies. We note a change in the trend of the dispersion curve at approximately 4 Hz, which is captured by the data predictions and is likely caused by a significant seismic impedance contrast beneath the site.

Table 2. Model parameter prior bounds.

Parameter	Site A		Site B	
	min	max	min	max
depth 1 (m)	5	50	5	50
depth 2 (m)	5	200	5	200
V_S1 (m/s)	100	750	100	750
V_S2 (m/s)	200	1250	200	1000
V_S3 (m/s)	500	3000	750	3000

We performed probabilistic inversions assuming several possible numbers of layers in the 1D V_S model. We note that results from these various inversions yield similar results. Qualitatively, we identify that a model consisting of three layers (two layers over a half-space) is the simplest model that can explain the data. The result of our probabilistic inversion at site A is displayed in Figure 4c and 4d. Specifically, we illustrate the marginal posterior density of V_S as a function of depth, as well as the marginal probabilities for layer interface depths. The inversion results provide evidence for a layer with V_S between 200 and 225 m/s, to a depth of around 20 m (between 15 and 22 m). The second layer has much larger uncertainty in both velocity and interface depth. Our results indicate a large contrast in V_S between the first and second layers and a gradual, monotonically increasing V_S below the first layer. The second interface depth ranges between 27 and 95 m, and inferred V_S values range between 325 and 850 m/s. Beyond approximately 100 m depth, V_S continues to increase, but with a significant increase in V_S uncertainty. This provides some evidence of higher velocities at depth below site A, but that V_S values at these depths are likely beyond the resolution limits of our measurements.

Figure 5 displays the results of our passive seismic analysis for the data collected at site B. As with site A, the figure bounds indicate the most pertinent region of the model and do not reflect the entire allowable prior model space. The configuration of the passive seismic array is delineated in Figure 5a, which highlights the extent (aperture) and configuration of the instruments deployed at the baseball field site. Similarly to site A, we note that the minimum and maximum instrument separation distances are approximately 5 and 100 m, respectively. Figure 5b indicates the fit between the measured and predicted phase velocity dispersion data. Generally, for high frequencies, the data predictions fall within the error bars for the field observations. However, the low frequency data predictions do not fall within the observed data error bars and indicate a systematic bias with under-prediction of phase velocities. The errors are larger for frequencies less than around 2.5 Hz., and this is reflected in the larger range in data predictions for low frequencies. The under-prediction of phase velocities at low frequencies suggests that the measured data require higher velocities than our model assumptions permit. Future work will further investigate the cause of this bias and the V_S values required to fit the data, and the plausibility of such high V_S values.

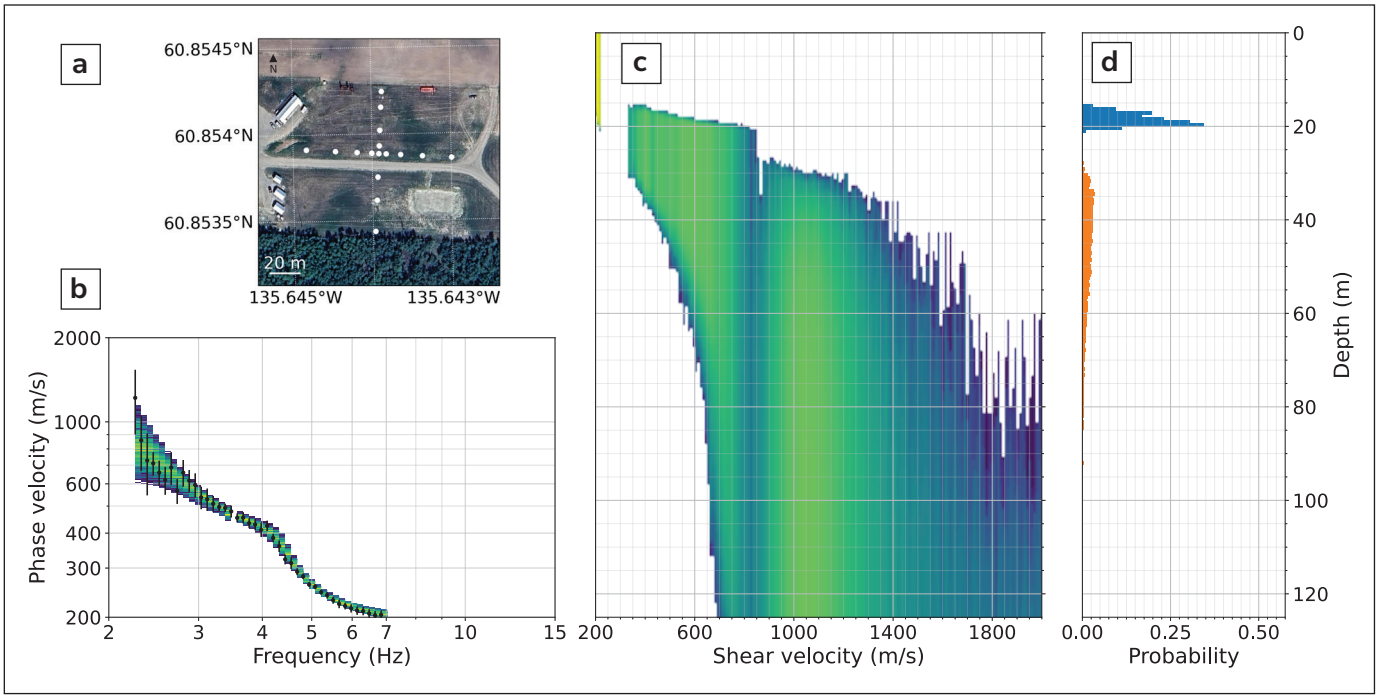

Figure 4. *Passive seismic analyses at site A.* ***(a)*** *Configuration of passive seismic array at site A.* ***(b)*** *Observed data (black markers with error bars) and predicted data (histogram); blue indicates low probability and yellow indicates high probability.* ***(c)*** *Marginal posterior probability density of shear-wave velocity (V_S) as a function of depth.* ***(d)*** *Marginal posterior probabilities for interface depths.*

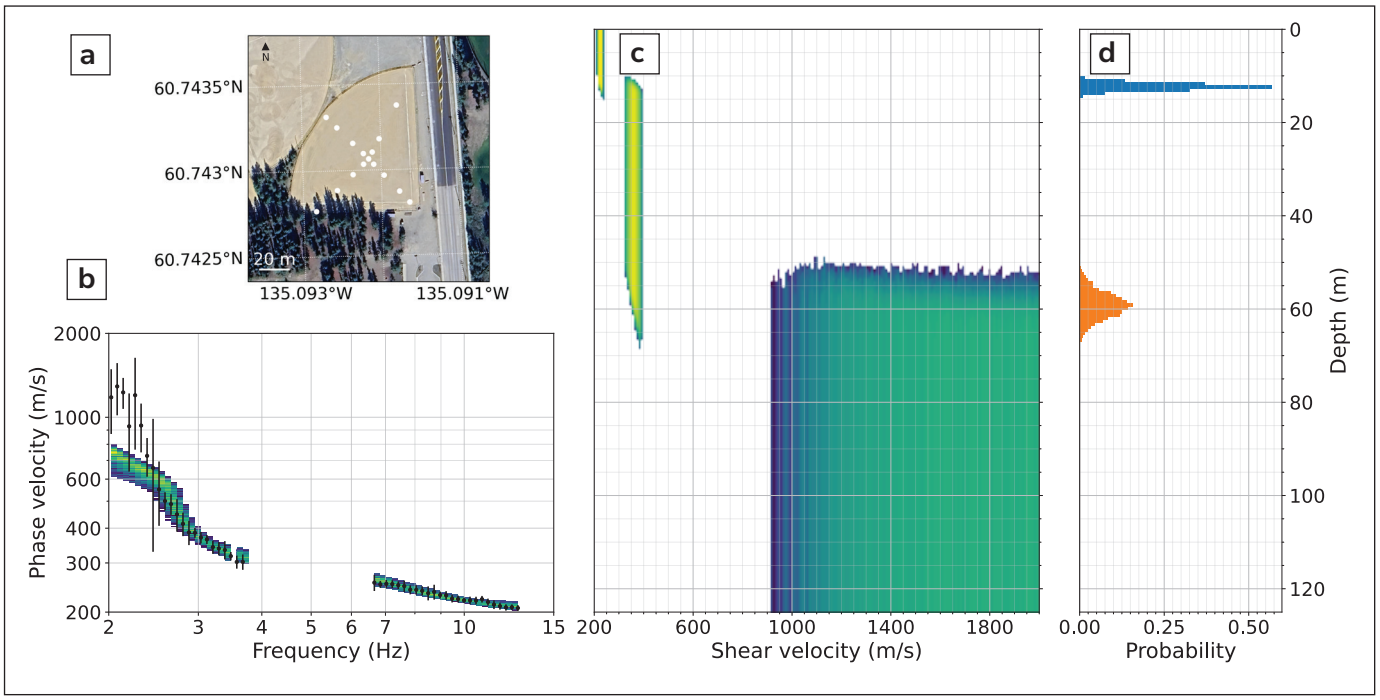

Figure 5. *Passive seismic analyses at site B.* ***(a)*** *Configuration of passive seismic array at site B.* ***(b)*** *Observed data (black markers with error bars) and predicted data (histogram); blue indicates low probability and yellow indicates high probability.* ***(c)*** *Marginal posterior probability density of shear-wave velocity (V_S) as a function of depth.* ***(d)*** *Marginal posterior probabilities for interface depths.*

The result of our probabilistic inversion at site B is displayed in Figure 5c and 5d. As discussed above, we assume a model consisting of two layers over a half-space. Specifically, we illustrate the marginal posterior density of V_S as a function of depth, as well as the marginal probabilities for layer interface depths. The inversion results provide evidence for a layer with V_S between 200 and 250 m/s, to a depth between 10 and 15 m. The second layer has V_S between 320 and 400 m/s, and interface depth between 52 and 57 m. Beneath the second layer is an effectively unconstrained half-space, with the data supporting V_S above the upper prior bound of 3000 m/s.

Discussion and conclusions

This section considers seismic engineering parameters that are summarized in Fig 6. The time-average V_S of the uppermost 30 m beneath a site (V_{S30}) is an important seismic engineering parameter that is used to accurately apply the National Building Code of Canada. Typically, methods that infer or measure V_{S30} report a single value. In this work, the V_{S30} values are computed for the ensemble of McMC models to obtain a posterior distribution of the V_{S30} values (Fig. 6a). This distribution quantifies the uncertainty of the V_{S30} results. Based on the values of V_{S30}, the site classification for both sites is D, stiff soil. For site A, the most probable value of V_{S30} is ~275 m/s, and the values range between 249 and 280 m/s. For site B, the most probable value of V_{S30} is ~285 m/s, and the values range between 275 and 295 m/s. These results suggest a moderate amplification potential in Whitehorse, compared to a reference site typically assumed to have V_{S30} = 760 m/s (Kolaj et al., 2020). Recently, a similar site classification was performed for 14 sites in the Haines Junction (Dakwäkäda) area (Gosselin et al., 2025). Estimates of the amplification potential in the Haines Junction area are generally less than for Whitehorse. However, the two Whitehorse sites we consider in this study are located in relatively soft sediments for the region. An analysis of more sites is required to understand how widespread our inference of low near-surface V_S estimates is throughout the Whitehorse area.

For complex stratigraphy sites, in situations where there is an impedance contrast in the upper 30 m beneath a site, V_{S30} may underestimate the site hazard (Castellaro et al., 2008; Lee and Trifunac, 2010). Since we infer that both sites have an impedance contrast within the top 30 m, computing the time-average of the uppermost

10 m beneath a site (V_{S10}) may be more indicative of near-surface sediment rigidity (Fig. 6b). However, V_{S10} has no regulatory significance for the seismic hazard model. For site A, the most probable value of V_{S10} is ~210 m/s. Values range between 195 and 218 m/s. For site B, the most probable value of V_{S10} is ~222 m/s, and values range between 208 and 232 m/s. Site B has velocities about 10 m/s faster than site A for both V_{S10} and V_{S30}. However, both sites have similar values that are nearly within their respective uncertainties. For both sites, the V_{S30}values are about 65 m/s faster than the V_{S10} values (Fig. 6), which illustrates how the V_{S30} values could under-predict seismic amplification hazard. The natural state of sediment rigidity at site B may be disrupted by the construction of the baseball diamond. The V_S of sediments beneath roads and other infrastructure can increase due to the changes in substrate sediment during contsruction (Gosselin et al., 2018). Yet, this effect is typically limited to the shallowest part of the subsurface and may not be resolved from our data due to the frequency band limitations in our measurement.

Limitations of this work include the assumption that Rayleigh-waves dominate the seismic ambient noise field on vertical-component recordings. The Earth is modelled as laterally homogeneous isotropic layers over the spatial extent of the array, which may not be accurate in an area with variable geology. Further, this assumption may not hold where sediment properties have a gradational change with depth, as results for site A suggest may be a possibility for depths greater than 20 m. The bandwidth for both sites is limited by the aperture and spacing of the array, which will influence the ability to resolve V_S in both the shallowest and deepest parts of the model. The results are also limited by the chosen f-k beamforming processing parameters, which allow only phase velocities between 200 and 2000 m/s. Furthermore, the probabilistic inversion depends on the assumption of the data error distribution. For this preliminary work, we assume independent, symmetric errors. The errors in the dispersion curves are likely covariant (Dettmer et al., 2012) at all frequencies and are asymmetric in the linear velocity space. Consequently, model uncertainty may be underestimated here.

Future work will include revisiting the f-k beamforming processing with wider velocity bounds to better constrain high frequencies, as well as investigating the

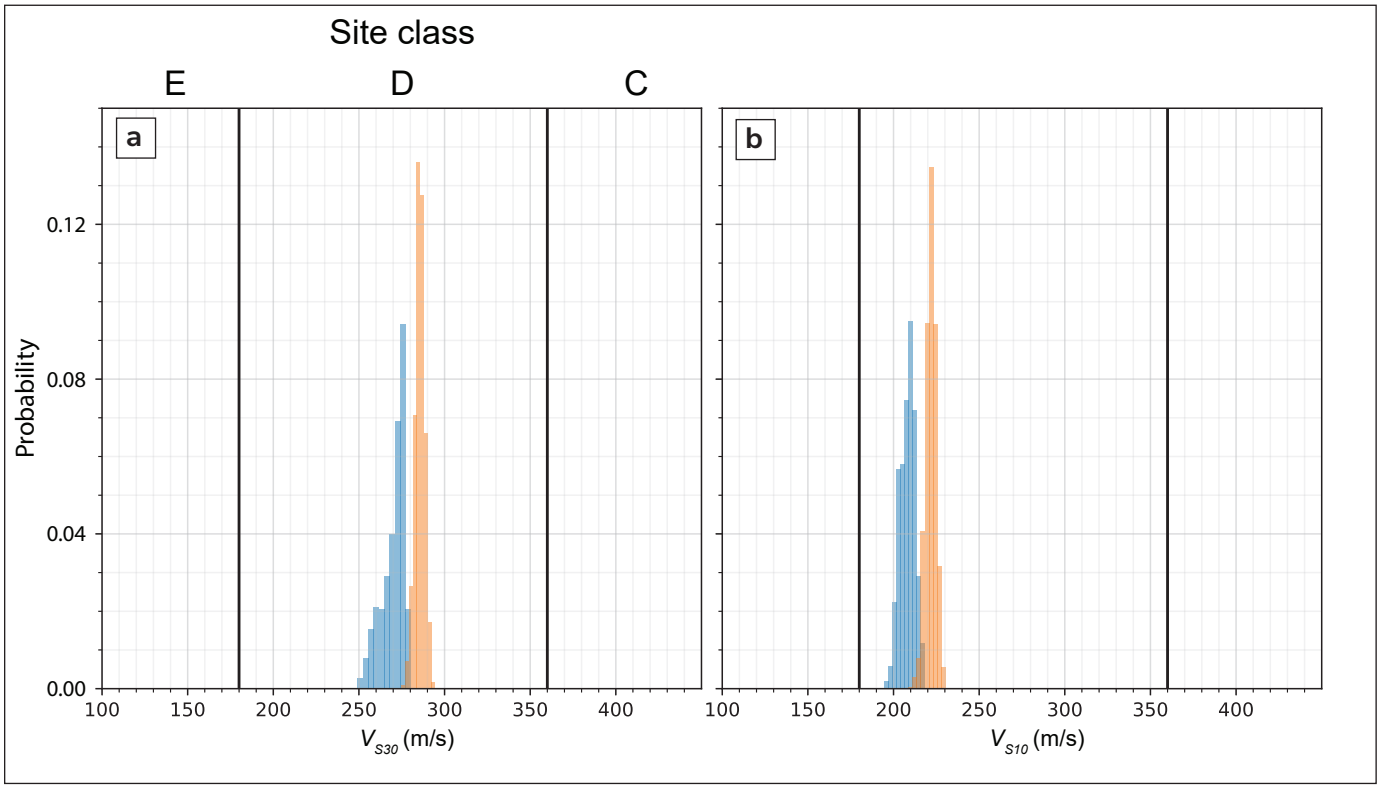

Figure 6. *Time-averaged velocity for* ***(a)*** *top 30 m (V_{S30}) and for* ***(b)*** *top 10 m (V_{S10}) for site A (blue) and site B (orange). Site classes are provided for V_{S30} where they are formally defined.*

under-prediction of phase velocities at low frequencies for site B. The under-prediction of low-frequency data implies that the data could require higher V_S values than allowed by the prior bounds, and so seismic resonances could be stronger than indicated by this initial model. We will also revisit the data error model, considering asymmetric and covariant data errors. Similar analysis will be performed for more sites throughout the Whitehorse area, incorporating additional data types (e.g., horizontal-to-vertical spectral ratios). Finally, we will extend the earthquake hazard analyses to consider site resonance, ground motion predictions and uncertainty quantification for all sites.

Although Whitehorse has no record of earthquakes in the immediate vicinity, it faces shaking hazards due to large earthquakes from the Aleutian subduction zone and moderate-sized earthquakes from closer, active faults. The larger and more distant earthquakes cause shaking at lower frequencies, while the moderate earthquakes cause shaking at higher frequencies. Characterizing shallow subsurface sediment conditions is important for understanding seismic wave amplification and resonance at local scales, and how the frequency content of various seismic sources may impact site-specific earthquake shaking. Furthermore, earthquake shaking can have implications for secondary hazards such as soil liquefaction or landslides. This work is important to understand the potential for landslide activation by shaking, particularly for the Whitehorse community. This preliminary research helps us better understand earthquake hazard for an understudied region, providing more information for the national hazard model, which has impacts for the community of Whitehorse, and other seismically active regions in Canada's North.

References

Anderson, J.G., Bodin, P., Brune, J.N., Prince, J., Singh, S.K., Quass, R. and Onate, M., 1986. Strong ground motion from the Michoacan, Mexico, earthquake. Science, vol. 233, no. 4768, p. 1043–1049.

Anderson, J.G., Lee, Y., Zeng, Y. and Day,S., 1996. Control of strong motion by the upper 30 meters. Bulletin of the Seismological Society of America, vol. 86, no. 6, p. 1749–1759, https://doi.org/10.1785/BSSA0860061749.

Bard, P.Y. and Bouchon, M., 1980. The two-dimensional resonance of sediment-filled valleys. Bulletin of the Seismological Society of America, vol. 75, no. 2, p. 519–541, https://doi.org/10.1785/BSSA0750020519.

Biegel, K.M., Gosselin, J.M., Dettmer, J., Colpron, M., Enkelmann, E. and Caine, J., 2024. Earthquake relocations delineate a discrete fault network and deformation corridor throughout southeast Alaska and southwest Yukon. Tectonics, vol. 43, no. 5, https://doi.org/10.1029/2023TC008140.

Blais-Stevens, A., Clague, J.J., Brahney, J., Lipovsky, P., Haeussler, P.J. and Menounos, B., 2020. Evidence for large Holocene earthquakes along the Denali fault in southwest Yukon, Canada. Environmental and Engineering Geoscience, vol. 26, no. 2, p. 149–166, https://doi.org/10.2113/EEG-2263.

Brideau, M.-A., Arenson, L.U., Porter, M., Mickey, A., Eshpeter, T. and Allen, T., 2024. The Whitehorse escarpment– preliminary landslide risk assessment. In: 77th Canadian Geotechnical Conference and the 16th Joint CGS/IAH-CNC Groundwater Conference, Montréal, QC, Canada.

Bruhn, R.L., Sauber, J., Cotton, M.M., Pavlis, T.L., Burgess, E., Ruppert, N. and Forster, R.R., 2012. Plate margin deformation and active tectonics along the northern edge of the Yakutat Terrane in the Saint Elias Orogen, Alaska, and Yukon, Canada. Geosphere, vol. 8, no. 6, p. 1384–1407, https://doi.org/10.1130/GES00807.1.

Castellaro, S., Mulargia, F. and Rossi, P.L., 2008. Vs30: Proxy for seismic amplification? Seismological research letters, vol. 79, no. 4, p. 540–543, https://doi.org/10.1785/gssrl.79.4.540.

Dettmer, J., Molnar, S., Steininger, G., Dosso, S.E. and Cassidy, J.F., 2012. Trans-dimensional inversion of microtremor array dispersion data with hierarchical autoregressive error models. Geophysical Journal International, vol. 188, no. 2, p. 719–734, https://doi.org/10.1111/j.1365-246X.2011.05302.x.

Doser, D. I., 2006. Relocations of earthquakes (1899–1917) in south-central Alaska. Pure and Applied Geophysics, vol. 163, no. 8, p. 1461–1476, https://doi.org/10.1007/s00024-006-0085-3.

Dutta, U., Yang, Z., Xu, G. and Haziribaba, K., 2008. Effect of seasonally frozen soil and permafrost on seismic site response. In: 14th World Conference on Earthquake Engineering, Beijing, China.

Eberhart-Phillips, D., Haeussler, P.J., Freymueller, J.T., Frankel, A.D., Rubin, C.M., Craw, P., Ratchkovski, N.A., Anderson, G., Carver, G.A., Crone, A.J., Dawson, T.E., Fletcher, H., Hansen, R., Harp, E.L., Harris, R.A., Hill, D.P., Hreinsdóttir, S., Jibson, R.W., Jones, L.M., Kayen, R., Keefer, D.K., Larsen, C.F., Moran, S.C., Personius, S.F., Plafker, G., Sherrod, B., Sieh, K., Sitar, N. and Wallace, W.K., 2003. The 2002 Denali fault earthquake, Alaska: A large magnitude, slip-partitioned event. Science, vol. 300, no. 5622, p. 1113–1118, https://doi.org/10.1126/science.1082703.

Finley, T., 2025. Neotectonics of major faults in the Canadian Cordillera. PhD thesis, University of Victoria, British Columbia, Canada, 151 p.

Finley, T., Nissen, E., Cassidy, J.F., Salomon, G., Leonard, L.J. and Froese, D., 2025. Large surface-rupturing earthquakes and a> 12 kyr, open interseismic interval on the Tintina fault, Yukon. Geophysical Research Letters, vol. 52, no. 14, https://doi.org/10.1029/2025GL116050.

Gardner, G., Gardner, L. and Gregory, A., 1974. Formation velocity and density—the diagnostic basics for stratigraphic traps. Geophysics, vol. 39, no. 6, p. 770–780, https://doi.org/10.1190/1.1440465.

Gosselin, J.M., Biegel, K.M., Dettmer, J., Gilbert, H., Colpron, M. and Enkelmann, E., 2024. Crustal stress near the Yakutat microplate collision from probabilistic earthquake focal mechanisms. Canadian Journal of Earth Sciences, vol. 62, no.4, p. 807–820, https://doi.org/10.1139/cjes-2024-0095.

Gosselin, J. M., Cassidy, J. F., Dosso, S. E. and Brillon, C., 2018. Probabilistic seismic-hazard site assessment in Kitimat, British Columbia, from Bayesian inversion of surface-wave dispersion. Canadian Geotechnical Journal, vol. 55, no. 7, p. 928–940, https://doi.org/10.1139/cgj-2017-0265.

Gosselin, J.M., Dettmer, J., Lipovsky, P. and Cronmiller, D., 2025. Seismic site amplification assessment in the Dakwäkäda (Haines Junction) area of Yukon, Canada, from probabilistic inference of passive seismic measurements. Canadian Geotechnical Journal, https://doi.org/10.1139/cgj-2025-0357.

Gosselin, J.M., Dosso, S.E., Askan, A., Wathelet, M., Savvaidis, A. and Cassidy, J.F., 2022. A review of inverse methods in seismic site characterization. Journal of Seismology, vol. 26, no. 4, p. 781–821.

Government of Yukon, 2022. Assessing climate change: Risk and resilience in the Yukon. Main Report, Government of Yukon, Whitehorse, 126 p, https://yukon.ca/sites/default/files/env/env-assessing-climate-change-risk-resilience-yukon-main-report.pdf.

Herrmann, R.B., 2013. Computer programs in seismology: An evolving tool for instruction and research. Seismological Research Letters, vol. 84, no. 6, p. 1081–1088, https://doi.org/10.1785/0220110096.

Hyndman, R., Cassidy, J., Adams, J, Rogers, G. and Mazzotti, S., 2005. Earthquakes and seismic hazard in the Yukon-Beaufort-Mackenzie. CSEG Recorder, vol. 30, no. 5, p. 32–67, https://www.seismescanada.rncan.gc.ca/hazard-alea/north-nord/Recorder_article.pdf.

Kellett, D., Ryan, J., Colpron, M., Zagorevski, A., Joyce, N., Zwingmann, H. and Kislitsyn, R., 2017. Report of activities, 2017, for Yukon tectonic evolution–late Mesozoic to Tertiary: GEM2 Cordillera project. Geological Survey of Canada Open File, vol. 8306, p. 14, https://publications.gc.ca/collections/collection_2018/rncan-nrcan/m183-2/M183-2-8306-eng.pdf.

Kolaj, M., Adams, J. and Halchuk, S., 2020. The 6th generation seismic hazard model of Canada. *In:* 17th World Conference on Earthquake Engineering, Sendai, Japan.

Lee, V.W. and Trifunac, M.D., 2010. Should average shear-wave velocity in the top 30 m of soil be used to describe seismic amplification? Soil Dynamics and Earthquake Engineering, vol. 30, no. 11, p. 1250–1258, https://doi.org/10.1016/j.soildyn.2010.05.007.

Lipovsky, P.S., 2023. Surficial geology and geohazards of the greater Whitehorse area. Yukon Geological Survey, Open File 2023-1, 67 p. plus appendices.

Luu, K., 2024. disba. https://pypi.org/project/disba/, [accessed 05/12/2025].

Molnar, S., Dosso, S.E. and Cassidy, J.F., 2010. Bayesian inversion of microtremor array dispersion data in southwestern British Columbia. Geophysical Journal International, vol. 183, no. 2, p. 923–940, https://doi.org/10.1111/j.1365-246X.2010.04761.x.

Nelson, J., Colpron, M. and Goodfellow, W., 2007. Tectonics and metallogeny of the British Columbia, Yukon and Alaskan Cordillera, 1.8 Ga to the present. In: Mineral Deposits of Canada: A Synthesis of Major Deposit Types, District Metallogeny, the Evolution of Geological Provinces, and Exploration Methods, Geological Association of Canada, Mineral Deposit Division, Special Publication 5, p. 755-791, https://cmscontent.nrs.gov.bc.ca/geoscience/publicationcatalogue/External/EXT060.pdf.

Plafker, G., 1970. Tectonics of the March 27, 1964, Alaska earthquake. US Government Printing Office, Washington, D.C., 74 p., https://doi.org/10.3133/pp543I.

Proulx, M., 2022. Road likely closed for days while city assesses risk after landslide, Whitehorse mayor says. CBC News, https://www.cbc.ca/news/canada/north/whitehorse-landslide-may-1-1.6437720, [accessed 05/12/2025].

Sun, H., Niu, F., Zhang, K. and Ge, X., 2017. Seismic behaviors of soil slope in permafrost regions using a large-scale shaking table. Landslides, vol. 14, no. 1, p. 1513–1520, https://doi.org/10.1007/s10346-017-0823-x.

van Drecht, L.H., Beranek, L.P., Colpron, M. and Wiest, A.C., 2022. Development of the Whitehorse trough as a strike-slip basin during early to middle Jurassic arc-continent collision in the Canadian Cordillera. Geosphere, vol. 18, no. 5, p. 1538–1562, https://doi.org/10.1130/GES02510.1.

Wathelet, M., Chatelain, J.-L., Cornou, C., Giulio, G.D., Guillier, B., Ohrnberger, M. and Savvaidis, A., 2020. Geopsy: A user-friendly open-source tool set for ambient vibration processing. Seismological Research Letters, vol. 91, no. 3, p. 1878–1889, https://doi.org/10.1785/0220190360.

Wathelet, M., Jongmans, D., Ohrnberger, M. and Bonnefoy-Claudet, S., 2008. Array performances for ambient vibrations on a shallow structure and consequences over VS inversion. Journal of Seismology, vol. 12, no. 1, p. 1–19.

White, D., Colpron, M., Buffett, G. and Lane, L., 2012. Seismic and geological constraints on the structure and hydrocarbon potential of the northern Whitehorse trough, Yukon, Canada. Bulletin of Canadian Petroleum Geology, vol. 60, no. 4, p. 239–255, doi:10.2113/gscpgbull.60.4.2.

Witter, J.B., 2025. Analysis of geoscience data for geothermal exploration in the Whitehorse area, Yukon. Yukon Geological Survey, Government of Yukon, Open File 2025-8, 53 p. plus appendices.

Xia, J., Miller, R.D. and Park, C.B., 1999. Estimation of near-surface shear-wave velocity by inversion of Rayleigh waves. Geophysics, vol. 64, no. 3, p. 691–700, https://doi.org/10.1190/1.1444578.